electronic reprint

Acta Crystallographica Section B
Structural Science
ISSN 0108-7681

The self-hosting structure of β-Ta

Alla Arakcheeva, Gervais Chapuis and Vladimir Grinevitch

Acta Crystallographica Section B
Structural Science
ISSN 0108-7681

The self-hosting structure of β-Ta

Alla Arakcheeva,[a,b] Gervais Chapuis[a]* and Vladimir Grinevitch[b]

[a]Institute of Crystallography, University of Lausanne, BSP, 1015 Lausanne, Switzerland, and [b]Baikov Institute of Metallurgy RAS, 117334 Moscow, Russia

Correspondence e-mail: gervais.chapuis@ic.unil.ch

Received 6 June 2001
Accepted 22 October 2001

Using electrodeposition from a bath of molten fluorides, single crystals of tetragonal β-tantalum have been obtained for the first time at normal pressure. The unit-cell parameters are a = 10.211 (3), c = 5.3064 (10) Å, space group $P\bar{4}2_1m$. The β-Ta structure belongs to the σ-type Frank–Kasper structures which are typical for binary intermetallic compounds and β-U. In comparison to the σ-type, additional intercalated Ta atoms (population factor ~0.01) have been detected between the atoms located in the channels of the structure. The shorter interatomic distances observed between the channel atoms in comparison with the atoms of the framework justify the 'self-hosting' characteristic. β-Ta exhibits common features with the complex tetragonal structures of the high-pressure phases for the elements Rb, Ba, Sr, Bi and Sb.

1. Introduction

The tetragonal β-Ta phase is absent in the pressure–temperature (P–T) phase diagram of Ta (Young, 1991). According to the data currently available, only β-Ta powder could be produced by electrolysis (see Moseley & Seabrook, 1973, and references cited therein). High temperature (~1000 K) and the presence of an electrical field under reducing conditions allows the formation of β-Ta by electrolytic crystalization on a cathode. Thin films (up to 30 nm) of this phase used as an underlying layer for Cu metallization can also be obtained by dirrect current (*d.c.*) magnetron sputtering (Westwood, 1970; Kwon *et al.*, 1997; Lee *et al.*, 1999). β-Ta was first obtained by *d.c.* magnetron sputtering (Mills, 1966; Read & Altman, 1965) and later by electrodeposition from a molten fluoride bath at 1073 K (Moseley & Seabrook, 1973). The CrFe-type structure (so-called Frank–Kasper σ-phase structures of binary compounds; Frank & Kasper, 1958, 1959; space group $P4_2/mnm$) and unit-cell parameters [a = 10.194 (3), c = 5.313 (2) Å] of β-Ta were reported on the basis of powder diffraction data (Moseley & Seabrook, 1973). According to this reference, β-Ta and β-U (Donohue & Einspahr, 1971) are isomorphous. However, in view of the uncertainty concerning the details including the space group of β-U (the best reliability factor reported was R = 0.24; Donohue & Einspahr, 1971), the same article (Moseley & Seabrook, 1973) mentioned that an accurate assessment of the positional parameters would only be possible on the basis of single-crystal diffraction data.

Using electrolytic crystallization, we have succeeded in obtaining very small (~ 5–20 μm) single crystals of β-Ta. A

recent investigation of the complex tetragonal structures of the high-pressure (HP) phases of the group V metals Bi^{III}, Sb^{II} and As^{III} (McMahon, Degtyareva & Nelmes, 2000), with β-Ta related to the HP Ba^{IV}-type incommensurate structure (Nelmes *et al.*, 1999), has reinforced our interest in the tetragonal β-Ta phase.

In this article, we present the synthesis and structural data of β-Ta refined for the first time on the basis of single-crystal X-ray diffraction data obtained at room temperature and normal pressure.

2. Experimental

2.1. Synthesis

The light grey metallic formation of the β-Ta phase did grow on a cathode during the electrolysis of fluoride or oxofluoride melts with metallic Ta or TaO soluble anodes. K_2TaF_7 or K_2TaOF_5 was used as a Ta-containing component for the electrolyte. The ternary eutectic LiF–NaF–KF was used as a solvent. The electrolysis was carried out with temperature ranging from 893 to 1173 K and a cathode current density of 0.1–0.3 A cm^{-2} under an atmosphere of high purity argon. The electrolytic cell consisted of a glassy carbon crucible containing 50 g of molten electrolyte. The anode material was located on the bottom of the crucible. The Mo and Cu plate cathode was placed in the center of the cell. After completion of the electrolysis cycle, the cathodic plate and its deposit were cooled in an argon atmosphere. Finally, the cathode product was washed free of the entrapped salt phase with HCl water solution. Cubic α-Ta metal was deposited together with tetragonal β-Ta phase from the fluoride bath. With oxygen-containing melts, the cubic bronze $KTa_{1+z}O_3$ (Arakcheeva *et al.*, 2001) and tetragonal Ta-bronze (Arakcheeva *et al.*, 2000) also crystallize along with the β-Ta phase. The oxygen-free Ta phases have been obtained using an oxygen-free electrolytic bath (K_2TaF_7 with fluoride solvent), together with a Ta anode. The presence of O and F in the Ta phases was checked by two methods: increasing the probe weight after full oxidation and microprobe analysis. The β-Ta crystal used in the present X-ray study does not contain more than 0.001 at.% oxygen and fluorine.

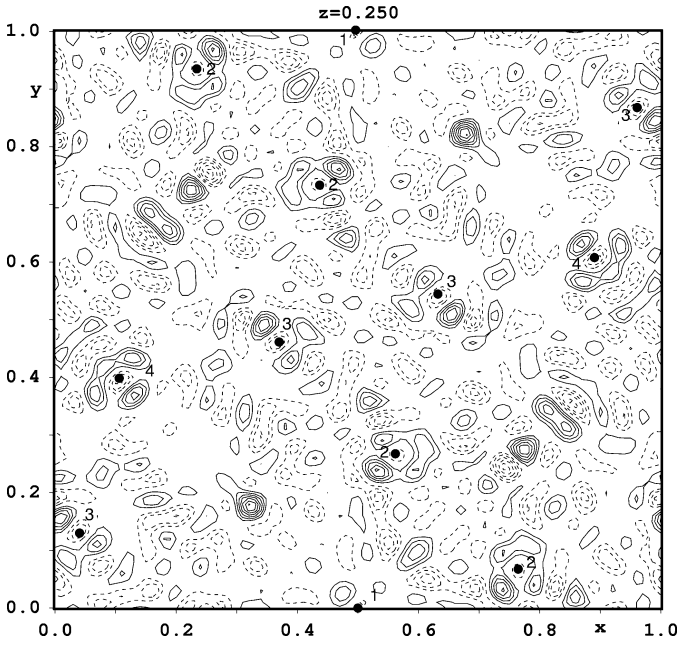

Figure 1
Residual electron density section for the β-Ta structure calculated from a refinement with six Ta atoms with isotropic thermal displacements using high-angle reflections ($665F$ with $\sin\theta/\lambda > 0.7$). Black circles and numbers indicate the positions of Ta atoms. The maxima located near the Ta positions justify the anharmonic approximation approach for the thermal atomic displacements. The increment between lines is 3 e $Å^{-3}$. Solid and dashed lines indicate positive and negative electron density, respectively.

2.2. X-ray measurements and structure refinement

A very small (~20 μm) isometric crystal sample obtained from a fluorine bath was chosen for the crystal structure investigation. The KM-4 CCD diffractometer (Mo $K\alpha$ radiation; tube voltage 55 kV; filament current 45 mA; KM-4 CCD/SAPPHIRE detector, sample–detector distance 51.7 mm, 829 frames) was used for the data collection [15 963 reflections with $I > 1.17\sigma(I)$; 7874 $I > 3\sigma(I)$; in a hemisphere of reciprocal space; $\sin\theta/\lambda < 1.1079$]. No satellites pointing to an incommensurate structure were observed in the reciprocal space. Structural amplitudes were corrected for absorption (μ = 147.48 mm^{-1}) for a spherical crystal. The tetragonal unit-cell parameters [a = 10.211 (3); c = 5.3064 (10) Å] were refined from 2054 reflections with $I > 7\sigma(I)$. The only systematic absence of reflections ($h00$, $h \neq 2n$) pointed to the space group $P\bar{4}2_1m$ rather than the $P4_2/mnm$ reported in Moseley & Seabrook (1973). Reflections $00l$ with l = 1, 7 [$I > 5\sigma(I)$] and l = 3, 5, 9 [$I > 3\sigma(I)$] are not compatible with the space group $P4_2/mnm$, which is pseudo-symmetric. The averaging of equivalent measurements was performed for the non-centrosymmetric point group $\bar{4}2m$ [R_{av} = 0.1449/0.1345/0.1284 for the $3114F > 1.17\sigma(F)$/$1769F > 3\sigma(F)$/$1398F > 5\sigma(F)$, respectively]. The high values of R_{av} are connected with the deviation from the regular sphere and the high absorption factor.

Taking into account the high values of R_{av}, only the strongest unequal reflections [$1398F > 5\sigma(F)$] were used for the refinement. This number yields the reflections-to-parameters ratio 6.08. The use of weaker reflections could result in a lower accuracy of the refinement. The full-matrix refinement based on F with anharmonic thermal displacement (Gram–Charlier expansion up to 5th rank) was performed for six Ta atomic positions yielding R = 0.0566 {wR = 2.98; weighting scheme $w = 1/[\sigma^2(F) + 0.0001F^2]$; GOF = 3.88; residual electron density $\Delta\rho_{max}$ = 19.99, $\Delta\rho_{min}$ = −11.39 e $Å^{-3}$}. The extinction coefficient 0.00150 (13) was obtained with the Becker–Coppens (*B-C*) type 1 Gaussian isotropic approximation (Petricek & Dusek, 2001). The anharmonic thermal displacement approach is based on the analysis of the different electron-density maps (Fig. 1), which were calculated from the refinement of six Ta positions with isotropic thermal displacements using high-angle reflections [$665F$ with $\sin\theta/\lambda > 0.7$; R =

0.0735, $wR = 0.0648$; GOF = 2.80; $\Delta\rho_{min} = -15$ e Å^{-3}; $\Delta\rho_{max} =$ 21 e Å^{-3}] . As seen from Fig. 1, the maxima of $\Delta\rho$ (∼15–20 e Å^{-3}) are located in the vicinity of the Ta atoms at distances ∼0.5–0.7 Å. All these maxima kept their positions with $\Delta\rho \simeq 12$ e Å^{-3} also after refinement with anisotropic displacement coefficients [665F with $\sin\theta/\lambda > 0.7$; $R = 0.0661$, $wR = 0.0548$; GOF = 2.41]. They are successfully parameterized by the anharmonic tensors of Ta atoms. The residual electron density map (Fig. 2a) calculated from all reflections does not contain these maxima.

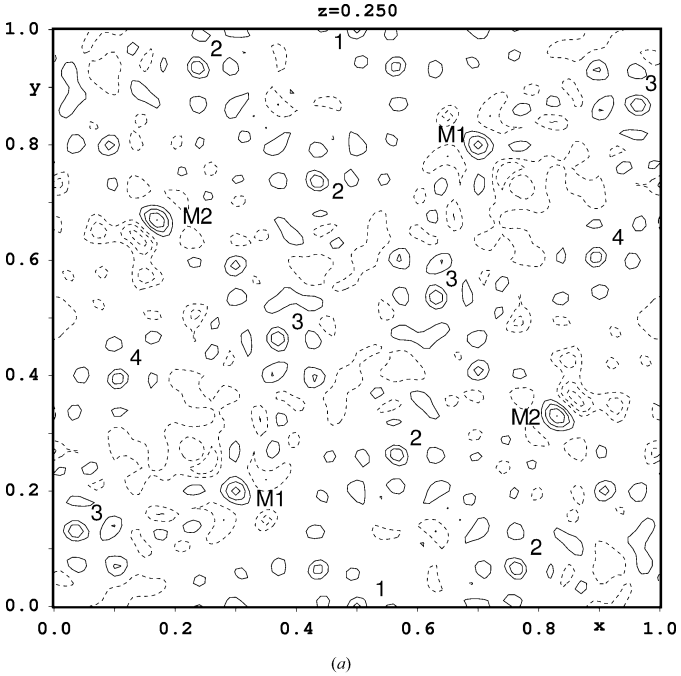

(*a*)

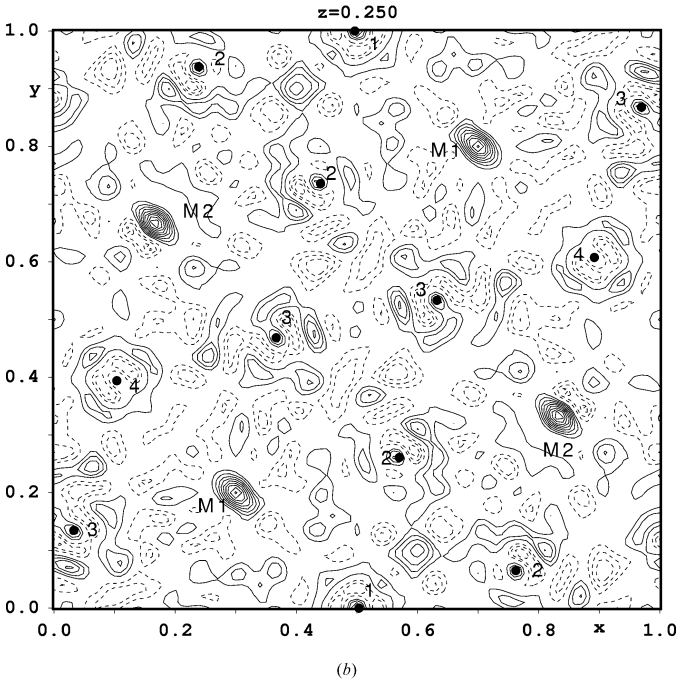

(*b*)

Figure 2
Residual electron density section $z = 1/4$ for the β-Ta structure calculated with (*a*) anharmonic and (*b*) anisotropic approximation of the atomic displacements. $M1$ and $M2$ indicate the highest maxima. The black circles and numbers indicate the positions of the Ta atoms. The increment between the lines is 2 e Å^{-3}. Solid and dashed lines indicate positive and negative electron density, respectively.

The final positional and equivalent isotropic displacement parameters are given in Table 1.[1] The population parameters of the six independent atomic positions were refined separately and did not deviate significantly from 1.

The two highest maxima ($M1$ and $M2$ in Fig. 2a) on the residual electron density ($\Delta\rho_{max} \simeq 20$ e Å^{-3}) are approximately twice the absolute value of the minimum ($\Delta\rho_{min} \simeq -10$ e Å^{-3}). These two maxima can have different origins. It could be due to the summation of waves attributed to the anharmonic displacements of Ta (terms higher than 5th ranks). This hypothesis is supported by the higher $M1$ and $M2$ maxima revealed on the residual electron density function calculated from a refinement with anisotropic thermal parameters (Fig. 2b) [1398F; $R = 0.0726$, $wR = 0.0388$; GOF = 5.08; $\Delta\rho_{min} = -21$ e Å^{-3}; $\Delta\rho_{max} = 38$ e Å^{-3}]. The second possibility could be due to the presence of a small amount of intercalated Ta_{int} atoms statistically distributed in the $M1$ and $M2$ positions (coherent defects of intercalation). This hypothesis is supported from a Fourier synthesis F(cal) calculated with the six basic Ta atoms where these maxima are absent. We plan some additional investigations of the β-Ta structure using synchrotron radiation at low temperature in order to clarify the origin of the residual density observed on the map. Including $M1$ and $M2$ as the Ta_{int} atom in the refinement leads, however, to a decrease in R to 0.0560 and a maximum residual $\Delta\rho$ of ∼12 e Å^{-3}. The refinement yields the position parameters $x_1 = 0.301$ (9), $y_1 = 0.199$ (9), $z_1 = 0.25$ (4) for $M1$ and $x_2 = 0.826$ (8), $y_2 = 0.326$ (8), $z_2 = 0.25$ (4) for $M2$, the population factors $p_1 = 0.009$ (4) and $p_2 = 0.011$ (4). The isotropic displacement factors have been fixed to $B = 1.0$.

All structural calculations were performed using the program *JANA*2000 (Petricek & Dusek, 2001).

3. Comparison of β-Ta with related structures

3.1. β-Ta as σ-phase

The crystal structure of the β-Ta phase (Fig. 3a) exhibits all the main features of a σ-phase (Frank & Kasper, 1958, 1959), in spite of reducing the symmetry from $P4_2/mnm$ to $P\bar{4}2_1m$. Two primary hexagonal–triangular Kagome nets $3636 + 3^26^2 + 6^3$(3: 2: 1) (according to the Pearson, 1972, notation) are located at $z \simeq 1/4$ and 3/4. They are formed by the atomic positions A, B, C and D according to the accepted notation given in Frank & Kasper (1958, 1959), see Table 1. According to the same notation, two secondary nets 3^2434 lie between the primary ones at $z \simeq 0$ and 1/2. The atoms of the secondary nets (E positions) are located on the axis of channels formed by the atoms of the primary net (Fig. 3a). The coordination polyhedra of all atoms are slightly deformed Frank–Kasper poly-

[1] Supplementary data for this paper are available from the IUCr electronic archives (Reference: OS0079). Services for accessing these data are described at the back of the journal.

Table 1
Atomic parameters in β-Ta, a Frank–Kasper σ-type structure; space group $P\bar{4}2_1m$; a = 10.211 (3); c = 5.3064 (10) Å.

Notation according to Frank & Kasper (1959) in the σ-type structure.

	Position	Notation	x	y	z	$U_{eq} \times 10^2$ (Å^2)
Ta1	2(*c*)	(*A*)	0.5	0	0.228 (2)	1.3 (1)
Ta2	8(*f*)	(*D*)	0.7598 (3)	0.0677 (3)	0.235 (1)	1.52 (7)
Ta3	8(*f*)	(*C*)	0.0343 (3)	0.1267 (4)	0.255 (2)	2.9 (1)
Ta4	4(*e*)	(*B*)	0.6033 (4)	0.1033 (4)	0.764 (2)	2.79 (7)
Ta5	4(*e*)	(*E*)	0.8142 (6)	0.3142 (6)	0.003 (1)	2.0 (1)
Ta6	4(*e*)	(*E*)	0.3196 (5)	0.1804 (5)	0.491 (1)	1.9 (2)

hedra [FKP*n*, *n* denoting the coordination number (CN)]: FKP12 for Ta1 (*A*) and Ta2 (*D*), FKP14 for Ta3 (*C*), Ta5 (*E*), Ta6 (*E*) and FKP15 for Ta4 (*B*).

The interatomic distances Ta—Ta in all FKPs [FKP12: average value is ⟨2.93⟩ Å with scattering 2.74–3.25 Å; FKP14: ⟨3.08⟩, 2.85–3.40 Å; FKP15: ⟨3.15⟩, 2.85–3.40 Å] are in good agreement with the Ta—Ta distances of the cubic *bcc* α-Ta phase stabilized at normal temperature and pressure (NTP) [8 × 2.86 Å and 6 × 3.31 Å with ⟨3.05⟩ Å for CN = 14], except for Ta5 and Ta6 (Table 2). The Ta5 and Ta6 atoms are located on the secondary nets (Fig. 3*a*) at 2.69 (1) Å, respectively 2.62 (1) Å from each other along the channel. These unusual short distances are ∼7% less than twice the tabulated metallic radius (1.43 Å) and practically equal to twice the tabulated (Emsley, 1991) covalent radius (1.34 Å) of Ta.

The channel of the β-Ta structure contains another surprising feature. The two highest maxima of the residual electron density mentioned above (*M*1 and *M*2 in Fig. 2) are located on the primary net (z = 1/4 and 3/4) close to the channel axis between Ta5 and Ta6 with a distance of approximately 1.4 Å between them.

According to Pearson (1972), the existence and structural stability of the commonly encountered binary intermetallic σ-phases are mainly controlled by geometrical parameters, one of them being the ratio of the atomic radii which should be close to 1.05. This ratio is responsible for the dissimilar and high coordination numbers. The valence electron concentration of approximately 6–7 e per atom is an essential feature of the σ-phases, also including β-U (Pearson, 1972). From this point of view, the specific features of the β-Ta phase in comparison with other σ-phases can be described as follows:

(i) β-Ta is a one-element structure, while all the others (except β-U) are binary intermetallic compounds from systems such as Cr–Fe, V–Ni, Nb–Re, Cr–Co and others (Pearson, 1972). In these binary compounds, the FKP15 contains the larger atom, while the FKP12 contains the smaller atom. This points to a probable differentiation of the electronic configuration for the different atomic positions in the β-Ta structure and therefore to different atomic radii.

(ii) In β-Ta, the valence electron concentration 5 e per atom is unusually small for a σ-phase including β-U. Taking into account the d^3s^2 valence electrons and the closeness of *f* and *d* electron levels, one can expect that the electrical field, high temperature and reducing conditions present during the β-Ta phase formation promotes the $f \rightarrow d$ transition, which is associated with the increase of the valence electron concentration.

(iii) The short interatomic distances between the channel atoms of the β-Ta structure mentioned above are not characteristic features of any σ-phase.

3.2. β-Ta and tetragonal HP metallic phases

On the other hand, the β-Ta structure exhibits common features with the complex tetragonal structures of the HP phases recently established for the elements Rb^{IV} (Schwarz *et al.*, 1999; McMahon *et al.*, 2001), Ba^{IV} (Nelmes *et al.*, 1999), Bi^{III}, Sb^{II} and As^{III} (McMahon, Degtyareva & Nelmes, 2000), and Sr^{IV} (McMahon, Bovornraranaraks *et al.*, 2000). The main characteristics of all these structure types are the high CNs of atoms and a differentiation of the atoms located in the *host* and *guest* sublattices. The guest atoms are placed in wide channels formed by the host atoms. Two examples from this group of structures are shown in Figs. 3(*b*) and (*c*) for comparison with the β-Ta structure (Fig. 3*a*). The channel atoms (the guest sublattices) differ from the host atoms: the shortening of Ta5—Ta6 distances and the possible intercalation of additional Ta_{int} atoms in the channels of the β-Ta structure were described above; in the HP phases, the guest structure is incommensurate with the host.

A comparison of β-Ta, the isomorphous β-U structures and the Rb^{IV}, Ba^{IV}, Bi^{III} related HP structures as opposed to the corresponding normal temperature and pressure (NTP) phases is represented in Table 2. The data related to the NTP phase structures were taken from Pearson (1972) and Emsley (1991). The relative atomic volume V/V_0, the interatomic distances and conditions of phase stabilization are extracted from the original articles (McMahon, Degtyareva & Nelmes, 2000; McMahon *et al.*, 2001; Nelmes *et al.*, 1999; Schwarz *et al.*, 1999) for the HP phase structures. For β-U these values were estimated on the basis of Donohue & Einspahr (1971). In the last case V and V_0 were calculated as the ratio (unit-cell volume/number of atoms in the unit cell) using β-U and the corresponding NTP phase data, respectively. For the alkaline (Rb) and rare-earth (Ba, Sr) elements, the pressure-driven partially completed process of the $s \rightarrow d$ transition is the stabilizing factor for the high-pressure complex tetragonal

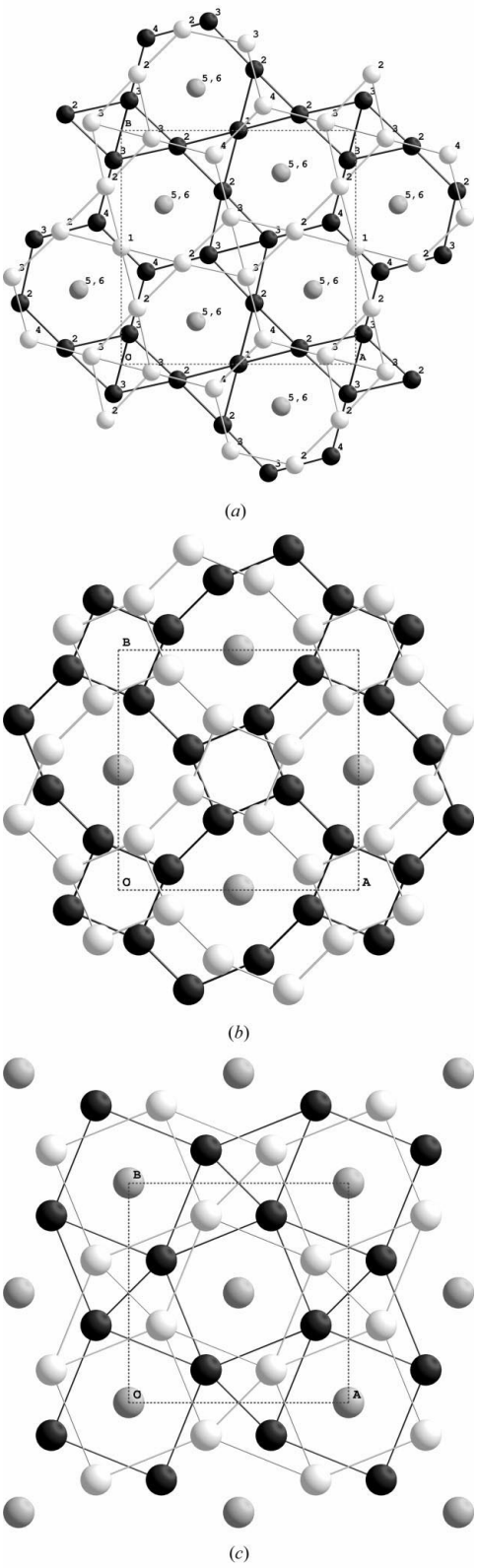

Figure 3
Crystal structures of (*a*) β-Ta, (*b*) HP-phase Rb^{IV} and (*c*) HP-phase Ba^{IV} projected along the *c* axis. The black and white circles indicate two consecutive levels of the primary atomic nets separated by 0.5*c* (host-sublattice). The grey circles indicate the channel atoms of guest sublattices. In (*a*) β-Ta the channel atoms form the secondary nets located halfway between the primary ones. In (*b*) Rb^{IV} and (*c*) Ba^{IV}, the guest sublattice is incommensurate with the host sublattice.

structure types (Schwarz *et al.*, 1999, and references cited therein; McMahon *et al.*, 2001; Nelmes *et al.*, 1999, and references cited therein; McMahon, Bovornraranaraks *et al.*, 2000). As a consequence, a decrease in interatomic distances and atomic volumes (see Table 2) is observed in the HP phases of the metallic elements. The CNs decrease slightly compared with the corresponding NTP phase.

In Sb and Bi, the pressure-driven increase of the space-filling degree leads to an overlap of the electron shells and the occurrence of mainly metallic bonds (Pearson, 1972). In the HP phases, the existence of some covalent bond components contributes to the presence of various atomic electron configurations. Compared with their NTP structure (see Table 2) we observe in the HP phase of Bi and Sb a decrease of the atomic volume and a convergence of the interatomic bonds.

The above analysis shows that the high pressure is a necessary condition for the complex tetragonal structure stabilization of the elements Rb, Ba, Sr, Bi and Sb, but for various reasons.

The NTP phase of uranium (an *f* element) exhibits a very low CN = 4 owing to complex electron interactions (Pearson, 1972). In β-U, the stable phase at high temperature, an increase of the average interatomic distances is observed along with an increase of the CNs. The atomic volume becomes slightly larger (see Table 2). The stability of this phase is due to the temperature-driven $5f \rightarrow 6d$ transitions, which results in various $5f^{4-n}6d^n7s^2$ electron configurations.

According to Moseley & Seabrook (1973), β-Ta irreversibly transforms to NTP α-Ta when heated above 1273 K. The high probability of the $4f \rightarrow 5d$ transition in β-Ta is supposed to be the stabilization factor of the σ-phase, which is induced at high temperature ($\sim$1000 K) by the electrical field and reducing conditions. The unusual condition for the β-Ta stabilization as opposed to β-U can be explained by the larger difference of energy between the 4*f* and 5*d* levels (β-Ta) than between 5*f* and 6*d* (β-U). The interatomic distances and CNs are practically the same in α-Ta and β-Ta; the atomic volume increases slightly in β-Ta (see Table 2). Additional investigations of the atomic electron configuration in both β-Ta and β-U must be provided to confirm the $f \rightarrow d$ transition.

It is worth pointing out the correlation between the atomic volume and the pressure conditions of the complex tetragonal structure stability. The lower limit of the high pressure at the phase transitions (and atomic contraction V_0/V_{HP}) increases with the atomic volume (V_0, NTP), which is linked to the higher number of electrons present in the shells of the atoms. The β-U and β-Ta phases are formed at normal pressure.

On the basis of this analysis (summarized in Table 2) and taking into account the existence of the HP phases Sb^{II} and As^{III} (McMahon, Degtyareva & Nelmes, 2000), isomorphous with Bi^{III} and Sr^{IV} (McMahon, Bovornraranaraks, 2000), isomorphous with Ba^{IV}, it can be concluded that the related complex tetragonal structure of the element is associated with the presence of *different electron types* in the outer atomic shell. The high and various CNs relate mainly to *metallic bonds* between atoms and *different electron configurations*, which is another necessary condition for the formation of

Table 2
Comparison of the related complex tetragonal structures of some elements.

Element *M*	Rb	Ba	Bi	Ta	U
Electronic configuration	$4p^6(4d^0)5s^1$	$5p^6(5d^0)6s^2$	$6p^35d^{10}6s^2$	$4f^{14}5d^36s^2$	$5f^46d^07s^2$
NTP phases					
Structure type	*bcc*	*bcc*	Deformed simple cubic (layer type)	*Bcc*	Strongly deformed *hcp*
$(M-M)_{NTR}$ (Å)	4.87, 5.62	4.34, 5.02	3.10, 3.47	2.86, 3.30	2.76, 2.85
CN	8 + 6 = 14	8 + 6 = 14	3 + 3 = 6	8 + 6 = 14	2 + 2 = 4
Atomic volume, V_{NTP} (Å^3)	88.75	63.44	35.28	18.01	20.75
Type of bond	Metallic bond	Covalent bonds in layer after Pearson (1972)	Covalent bonds in layer after Pearson (1972)	Metallic bond	Complex bonds after Pearson (1972)
Related tetragonal structures	HP phase	HP phase	HP phase	Electrolytic phase	HT phase
Phase Structure prototype	Rb^{IV} W_5Si_3 after Schwarz *et al.* (1999)	Ba^{IV} Al_2Cu after Nelmes *et al.* (1999)	Bi^{III} Bi_3In_5 after McMahon, Degtyareva & Nelmes (2000)	β-Ta Binary σ-phase	β-U Binary σ-phase
$(M-M)_H$ (Å); host-sublattice	$3.05 \div 3.26 \simeq 2R_{ion}$†	$3.38 \div 3.54 \simeq$ 20% less than $(M-M)_{NTR}$	$3.35 \div 3.51 \simeq (M-M)_{NTR}$	$2.75 \div 3.40 \simeq (M-M)_{NTR}$	$2.62 \div 3.71 \simeq (M-M)_{NTR}$
$(M-M)_G$ (Å); guest-sublattice located in channels	3.18 $\sim (M-M)_H$	3.41 $\sim (M-M)_H$	3.2 ~5% less than $(M-M)_H$†	2.62, 2.69 ~7% less than $(M-M)_H$;† (?) $1.4 = 2R_{ion}$†	2.70, 2.95 $\sim(M-M)_H$
CN	9_H, 6_G	11_H, up to 10_G	11_H, up to 10_G	12, 14, 15	12, 14, 15
V/V_0	0.29 ÷ 0.34	0.4 ÷ 0.5 (0.5 ÷ 0.67 for host sublattice)	0.79 ÷ 0.85	1.024	1.05
Condition of stability	$P = 17 \div 20$ GPa	$P = 12 \div 40$ GPa	$P = 3 \div 8$ GPa	Electrical field, $T \simeq 1000$ K, reducing conditions	$T = 934 \div 1045$ K
Factors of the structure type stabilization	Pressure-driven process of $s \rightarrow d$ transition ater Nelmes *et al.* (1999) and Schwarz *et al.* (1999)	Pressure-driven, mainly metal bonds accompanied by increase of CN	Electrical field and temperature driven $f \rightarrow d$ transition	Temperature-driven $f \rightarrow d$ transition	

† Common specific features for the β-Ta and the HP phase structures.

these phases. This conclusion confirms and completes the analogous suggestion of McMahon *et al.* (2001) concerning only the HP phases.

4. Discussion

4.1. Factors of the β-Ta structure stabilization

The calculated density of β-Ta is 16.28 g cm^{-3}. This is slightly less than 16.65 g cm^{-3} for the *bcc* α-Ta. Analysis of the specific features of β-Ta as a σ-phase points to a highly probable $f \rightarrow d$ electron transition. The density of the HP phase is expected to be larger than the density of the NTP phase. The radius of the $(n-1)f$ shell is less then the radius of the nd shell. Therefore, one might not expect the $f \rightarrow d$ transition to occur under pressure. Both facts suggest that β-Ta cannot occur as a HP phase. On the other hand, the channels in the β-Ta structure exhibit some characteristics of the HP phase. Taking into account the essential decrease of the interatomic distances in the HP phases of Ba^{IV} and Rb^{IV} (Table 2), owing to the pressure-driven $s \rightarrow d$ electron transition (Nelmes *et al.*, 1999; Schwarz *et al.*, 1999), the presence of a small amount of Ta_{int} atoms also with short interatomic distances (~1.4 Å = $2R_{ion}$ from Ta5 and Ta6) could be explained by the same electron transition process. The 7% shortening of the Ta—Ta distances between the guest–sublattice atoms Ta5 and Ta6 located in the channel is closely related to a similar structure, the high-pressure phase Bi^{III} where an analogous decrease of approximately 5% has been observed (McMahon, Degtyareva & Nelmes, 2000), see Table 2. In other related structures of HP phases, Rb^{IV} (McMahon *et al.*, 2001), Ba^{IV} (Nelmes *et al.*, 1999), as well as Bi^{III}, Sb^{II} and As^{III} (McMahon, Degtyareva & Nelmes, 2000), the incommensurate character of the channel atoms points to their relative independence. Note that according to Nelmes *et al.* (1999), the pressure dependence of the relative atomic volume is essentially weaker for the host sublattice than for the full structure of Ba^{IV} (see Table 2). This indicates that the atoms of the guest sublattice located in the channels can be more directly influenced by external pressure compared with other atoms in the structure. The shortening of the Ta—Ta distances between the atoms in the guest sublattice and the probable

intercalation of additional Ta_{int} atoms can be regarded as a local increase of the space filling within the channels of the β-Ta structure. A local increase of the space filling was also observed in the structural holes and channels of the perovskite-like cubic bronze $KTa_{1+z}O_3$ (Arakcheeva *et al.*, 2001) and in the hexagonal bronze $K_6Ta_{6.5+z}O_{15+x}F_{6+y}$ (Arakcheeva *et al.*, 2000), both produced by electrodeposition together with β-Ta from oxygen-containing melt. Approximately 2% of K atoms located in the holes of the $KTa_{1+z}O_3$ structure are statistically substituted by Ta–Ta dumb bells (Arakcheeva *et al.*, 2001). An intercalation of additional Ta_{int} atoms ~2.0 Å distant from the main K atoms and a substitution of one Ta atom by a Ta–Ta dumb bell were observed in the large hexagonal channels of the $K_6Ta_{6.5+z}O_{15+x}F_{6+y}$ structure. It is suggested that the local increase of the space filling in the channels and holes is due to the specific conditions (electrical field, high temperature and reducing conditions) used for the electrolytic crystallization in both β-Ta and the Ta-bronzes. This is reinforced by the fact that β-Ta could only be prepared in the presence of an electrical field. The deposition of diamond and diamond-like carbon nuclei (Sun *et al.*, 1999; Namba, 1992; Wang *et al.*, 1996; Tosin *et al.*, 1999) by electrolysis also seems to confirm the similarities of the effects of electrical crystallization and the external high pressure.

From the comparison of β-Ta with the σ and HP phases we can deduce that the $f \rightarrow d$ electron transition in β-Ta is usually associated with high temperature and cannot accompany a HP phase formation. The shortening of the interatomic distances between the channel atoms in β-Ta cannot be associated with the high temperature which usually accompanies an HP phase formation. This is why β-Ta is absent on the P–T phase diagram of Ta (Young, 1991).

A series of experiments on electrodeposition are currently performed at various temperatures (T) and cathode electrical current (E) in order to gain some insight into the α-Ta/β-Ta phase relation *versus* T and E.

We thank Drs H. Birkedal and Ph. Pattison for drawing our attention to the HP phases of Ba and Rb. We also thank Professors A. L. Udovskii, E. G. Polykov and V. F. Shamray for helpful discussion. We acknowledge the technical support from Dr M. Meyer and G. Lubman. This work is supported by the Russian Foundation for Basic Research (grant 98-03-32804) and by the Herbette Foundation of the University of Lausanne.

References

Arakcheeva, A., Chapuis, G., Grinevitch, V. & Shamray, V. (2001). *Acta Cryst.* B**57**, 157–152.
Arakcheeva, A., Grinevitch, V., Mitin, V. & Shamray, V. (2000). Late Abstracts, 19th European Crystallographic Meeting, p. 12. August 25–31, Nancy.
Donohue, J. & Einspahr, H. (1971). *Acta Cryst.* B**27**, 1740–1743.
Emsley, J. (1991). *The Elements*, 2nd ed. Oxford: Clarendon Press.
Frank, F. C. & Kasper, J. S. (1958). *Acta Cryst.* **11**, 184–189.
Frank, F. C. & Kasper, J. S. (1959). *Acta Cryst.* **12**, 483–488.
Kwon, K.-W., Ruy, C., Sinclair, R. & Simon Wong, S. (1997). *Appl. Phys. Lett.* **70**, 3069–3071.
Lee, H.-J., Kwon, K.-W., Ryu, C. & Sinclair, R. (1999). *Acta Mater.* **47**, 3965–3975.
McMahon, M. I., Bovornraranaraks, T., Allan, D. R., Belmonte, S. A. & Nelmes, R. J. (2000). *Phys. Rev. B*, **61**, 3135–3138.
McMahon, M. I., Degtyareva, O. & Nelmes, R. J. (2000). *Phys. Rev. Lett.* **85**, 4896–4899.
McMahon, M. I., Rekni, S. & Nelmes, R. J. (2001). *Phys. Rev. Lett.* **87**, 055501-1–055501-4.
Mills, D. J. (1966). *Can. Ceram. Soc.* **35**, 48–52.
Moseley, P. T. & Seabrook, C. J. (1973). *Acta Cryst.* B**29**, 1170–1171.
Namba, Y. J. (1992). *Vac. Sci. Technol. A*, **40**, 3368–3370.
Nelmes, R. J., Allan, D. R., McMahon, M. I. & Belmonte, S. A. (1999). *Phys. Rev. Lett.* **83**, 4081–4083.
Pearson, W. B. (1972). *The Crystal Chemistry and Physics of Metals and Alloys.* New York: Wiley.
Petricek, V. & Dusek, M. (2001). *The Crystallografic Computing System.* Institute of Physics Academy of Sciences of the Czech Republic, Praha.
Read, M. H. & Altman, C. (1965). *Appl. Phys. Lett.* **7**, 51–52.
Schwarz, U., Grzechnik, A., Syassen, K., Loa, I. & Hanfland, M. (1999). *Phys. Rev. Lett.* **83**, 4085–4088.
Sun, Z., Wang, X. & Sun, Y. (1999). *Mater. Sci. Eng. B*, **65**, 194–198.
Tosin, M. C., Peterlevitz, A. C., Surdutovich, G. L. & Baranauskas, V. (1999). *Appl. Surf. Sci.* **144–145**, 260–264.
Wang, H., Shen, M., Ning, Z., Ye, C., Cao, C., Dang, H. & Zhu, H. (1996). *Appl. Phys. Lett.* **69**, 1074–1078.
Westwood, W. D. (1970). *Thin Solid Films*, **6**, 307–320.
Young, D. A. (1991). *Phase Diagrams of the Elements.* Berkeley, CA: University of California Press.